JOURNAL OF MATERIALS SCIENCE 28 (1993) 2820–2826

Metal–ceramic functionally gradient material produced by laser processing

K. MOHAMMED JASIM*, R.D. RAWLINGS, D.R.F. WEST
Department of Materials, Royal School of Mines, Imperial College of Science, Technology and Medicine, London SW7 2BP, UK

A technique of injection with a powder feed of a mixture of metal + ceramic which combines the processes of laser alloying, cladding and injection, has been applied to study the feasibility of using a continuous wave CO_2 laser to produce a functionally gradient material. A 2 kW CO_2 laser has been used to produce, on a nickel alloy substrate, single alloy/clad tracks and three totally overlapping clad tracks using powder mixtures of Al–10 wt% SiC, Al–30 wt% SiC and Al–50 wt% SiC, respectively. The variation of composition and structure with position in the processed material has been investigated with reference to the effect of processing traverse speed and the powder feed rate.

1. Introduction

The performance of a component may be improved by isolating the main structural material from the environment by means of a coating. Because the coating material and the substrate typically have different physical and mechanical properties, failure of the system is commonly associated with the interface. To reduce the likelihood of failure at the coating–substrate interface, additional layers between the substrate and the surface coating are sometimes employed to improve performance, for example, the intermediate bond layer incorporated in plasma-sprayed thermal barrier systems. Even such complex coating systems still contain discrete layers with regions of discontinuity of composition, structure and properties. A new concept is currently receiving much interest, particularly in Japan; instead of coating a substrate, bulk components are envisaged with controlled progressive changes in structure and properties thereby alleviating the interfacial problems. Materials with such changes within the component section are termed functionally gradient materials (FGMs). Examples of functional gradient materials which have been studied include Ni–ZrO_2, NiCr–ZrO_2, Cu–TiB_2, Ti–TiN, Ni–NiO, SiC–C and Ti–TiC [1–3].

The methods so far used to produce FGMs have included chemical and physical vapour deposition, powder metallurgy, plasma spray and self-propagating high-temperature synthesis. All these methods have some draw-backs, for example, slow rate of chemical and physical vapour deposition, the limitations on size and shape of powder metallurgy and the small number of systems amenable to self-propagating synthesis. FGMs have considerable potential and rapid, flexible production routes are required.

High-power lasers, such as the CO_2 type, are already used in coatings technology making use of the advantageous features, namely a clean source of energy, high local heat input, non-contact heating, and rapid and flexible processing which is amenable to computer control. Monson *et al.* [4] have used a laser to produce a clad layer of variable composition as a function of distance along the surface of a substrate. However, it appears that systematic studies have not been reported on the production of controlled compositional gradients normal to a substrate surface over distances greater than those in typical coatings. The present paper reports for the first time exploratory experiments aiming to produce composition gradients of this type, i.e. to obtain FGMs.

The laser surface treatments most relevant to FGMs are cladding, and cladding incorporating injection of particles (e.g. of ceramic). Cladding involves the continuous feed of a powder of the coating material into a laser-generated molten pool of the material as the substrate is scanned relative to the beam. Normally the powder is fully melted and some alloying with the substrate occurs. Cladding has been employed to produce a wide range of substrate–coating combination, including yttria-stabilized zirconia (YSZ) and YSZ + alumina [5, 6].

With particle injection the particle size and the processing parameters must be selected so that the interaction time is insufficient to produce significant melting/solution of the particles. Thus a particle-reinforced metal matrix composite is produced on the surface of a metal substrate with a fine-scale matrix microstructure resulting from the rapid cooling [7–10]. In the same way as for cladding, the substrate is scanned with respect to the laser beam.

Cladding and injection can be combined in a single process; referred to here as cladding with particle injection. The powder feed consists of two or more species, with different melting points, typically the dominant one being a metal and the other a ceramic. The powder mixture is fed into the laser beam but only

* On leave from Scientific Research Council, Baghdad. *Present address*: P.O. Box, 9225, Kadhimiya, Baghdad, Iraq.

0022–2461

the low melting point material becomes completely molten and the other species (usually a ceramic) remains as small solid particles or partially dissolves. Cladding with particle injection therefore gives a surface layer consisting of a particle-reinforced composite. An example is the production of a Stellite matrix with SiC on a steel substrate [11].

In the work reported here the substrate was a nickel-based high-temperature alloy (Inconel 625). Aluminium was studied as a component for the functionally gradient region for its aluminide-forming capability with nickel. SiC was chosen as the ceramic for its potential for improving wear resistance when present in substantial volume fractions as a particulate. The aim was to achieve progressive increase in aluminium and SiC content as the functionally gradient region was built up on the substrate by several overlapping laser processed tracks. The use of a multicomponent alloy as the substrate rather than pure nickel leads to considerable microstructural complexity. Accordingly the exploratory investigation reported here does not deal in full detail with all the microstructural features; attention is directed towards the problems of establishing laser-processing conditions, particularly powder feed rate and interaction time, which will allow control of the compositional gradient involving dilution of the successive tracks and the solution of the ceramic particles.

2. Experimental procedure

A 2 kW continuous wave (CW) CO_2 laser was used at 2 and 1.7 kW laser power normally with a beam diameter of 5 mm, but some samples were produced with a 3 mm beam, and traverse speeds of the specimen relative to the laser beam of 1–22 mm s^{-1}. An argon gas flow through the laser nozzle provided some protection against contamination. The Inconel 625 alloy used as the substrate was of (nominal) composition (wt %) 22 Cr, 9 Mo, 3.5 Fe, 4 Nb, 0.3 Si, 0.1 Ti, 0.1 Mn, 0.4 Co, 0.05 C and ~60.55 Ni.

Plate samples of dimensions 60 mm × 40 mm × 15 mm were sand blasted and coated with a thin layer of carbon to improve absorptivity. Powder mixtures of aluminium with 10, 30 and 50 wt % SiC were used to produce single tracks with powder feed rates in the range 2–8 g min^{-1}. To produce functionally gradient material, three totally overlapped tracks were produced. The first was deposited from a premix of Al + 10 wt % SiC. A second track was deposited on to the first using a mixture of Al + 30 wt % SiC; the third track was deposited using an Al + 50 wt % SiC mixture. Measurements of track width and height were made at each stage and the microstructure examined using a scanning electron microscope (SEM) with energy X-ray analysis facilities (EDS).

3. Results and discussion

3.1. Single tracks

Before attempting to produce a FGM by fully overlapping laser tracks, it was necessary to determine the processing conditions for satisfactory production of single tracks of Al–SiC on the substrate. Most of this work was carried out on the Al–10 wt % SiC mixture with essential complementary tests on other powder compositions.

At moderate traverse speeds of ~4–12 mm s^{-1}, continuous tracks were produced; however, speeds of less than 2 mm s^{-1} resulted in discontinuous tracks and speeds greater than 12 mm s^{-1} gave insufficient cladding. The values of track width and height above the substrate for a feed rate of 4 g min^{-1} and traverse speeds in the range 1–22 mm s^{-1} are presented in Fig. 1. Most of the data show a decrease in both dimensions with increase in traverse speed, which is consistent with previous work on alloying and cladding (e.g. [12, 13]). The exception to this trend is the reduction in track width at the slowest speed studied. This reduction is attributed to the high mass of feed per unit length of track, i.e. high value of feed rate/traverse speed (g mm^{-1}). The use of this parameter, values of which are given in Table I, is preferable to that of feed rate alone. The high mass of powder per unit length at slow traverse speeds restricts laser heating of the substrate and so reduces the extent of substrate melting. Interaction between the molten powder and the molten substrate becomes limited, leading to discontinuous tracks of narrow width but considerable height.

The tracks produced with Al–10 wt % SiC showed a tendency to be greater in height and slightly wider

TABLE I Area dilution of single track of Al–10 wt % SiC (4 g min^{-1} feed rate)

Traverse speed (mm s^{-1})	Area dilution (%)	Mass feed (feed/length) (g mm^{-1})
1	3	0.067
2.2	15	0.030
3.9	25	0.017
5.1	40	0.013
7.1	70	0.009
13.2	70	0.005

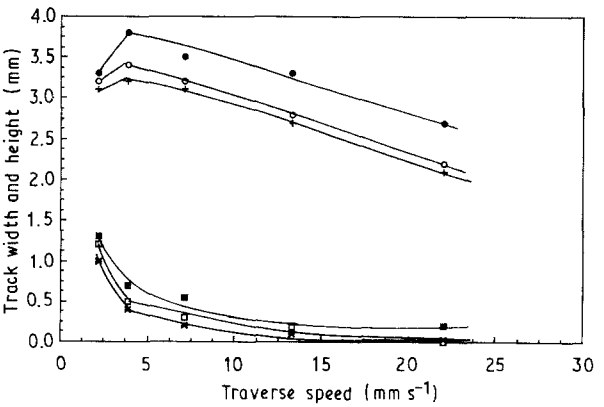

Figure 1 The relationship between track width and track height as a function of traverse speed, 2 kW laser power, 5 mm beam diameter and 4 g min^{-1} feed rate. Height of: (●) Al–10 wt % SiC, (○)Al–30 wt % SiC, (+) Al–50 wt % SiC. Width: (■) Al–10 wt % SiC, (□) Al–30 wt % SiC, (×) Al–50 wt % SiC.

than those for the higher SiC contents. This may be due to less melting of the powder as the proportion of the high melting point, high heat capacity SiC increases (the heat capacity of SiC is greater than for most metals but is slightly less than that of aluminium). The width at all speeds is less than the beam diameter (5 mm) and only a small increase in width is observed on increasing the beam diameter from 3 mm s^{-1} to 5 mm s^{-1}. This relative insensitivity of width to beam diameter is thought to be a consequence of the powder partially shielding the substrate from the laser beam.

Dilution in laser processing may be defined in terms of either the ratio of area of substrate melted to the total melted zone (substrate + clad layer) or, if the total melt zone is reasonably homogeneous, by comparing the chemical compositions of the powder and the melt zone [14]. In the present case, because of the large number of elements in the substrate and powder, measurement of dilution by composition is complex and therefore only area dilution values are given (Table I). It can be seen from Table I that the area dilution is very small at the low speed as a result of the high mass of feed per unit length which restricts heating of the substrate. Dilution reaches a maximum (~70%) at high speeds.

Fig. 2 illustrates the structure of the Al–10 wt % SiC track produced at ~4 g min^{-1} feed rate and 7 mm s^{-1} traverse speed; this is associated with very substantial dilution and complete solution of SiC. No other carbides were detected by the SEM examination. The average composition of the melt zone is given in Table II; note that carbon should be present in the processed zone as a result of the solution of SiC, but EDS cannot detect this element, therefore the element has been taken to be equal to the silicon content in atomic per cent. The composition of the grey dendritic-shaped areas is also given in Table II; these are nickel and aluminium rich (~48 at % Ni and 40 at % Al) in comparison with the average composition (including the interdendritic (light) areas. The high nickel and aluminium contents and lower chromium and molybdenum contents, of the dendrites indicate that these are based on β-NiAl phase. From comparison with the average composition data it is deduced that the interdendritic regions are relatively low in aluminium and high in chromium and molybdenum. This structure was typical of that obtained at most feed rates and traverse speeds with the Al–10 wt % SiC powder. Only at high feed rates and low speeds, e.g. 6 g min^{-1} and 2.2 mm s^{-1}, were some undissolved SiC particles and needle-like particles, interpreted as Al_4C_3 present (Fig. 3). The amount of aluminium carbide increases with increase in the traverse speed above 2.2 mm s^{-1} up to 7.1 mm s^{-1}. Clearly, due to solution of the SiC, successful injection is difficult when using powders with low SiC content.

Using a mixture of Al–30 wt % SiC to produce tracks, it was possible to achieve injection of the SiC particles without complete solution. Fig. 4 shows a sample processed at a feed rate of 5 g min^{-1} and 1 mm s^{-1} traverse speed with 3 mm beam diameter; the distribution of SiC was not uniform. Experiments with speeds of 2.2 and 7 mm s^{-1} produced samples with substantial volume fractions of undissolved SiC particles; the matrix regions were aluminium rich (aluminium content of ~ 90 wt %). The microstructure was complex with regions of eutectic appearance together with particles of intermetallic compounds; some of the latter as analysed by EDS contained ~22–25 at % Ni and 70–75 at % Al, suggesting that the phase is $NiAl_3$, and other particles contained aluminium, chromium, molybdenum and nickel (Table III). Conditions for particle injection were

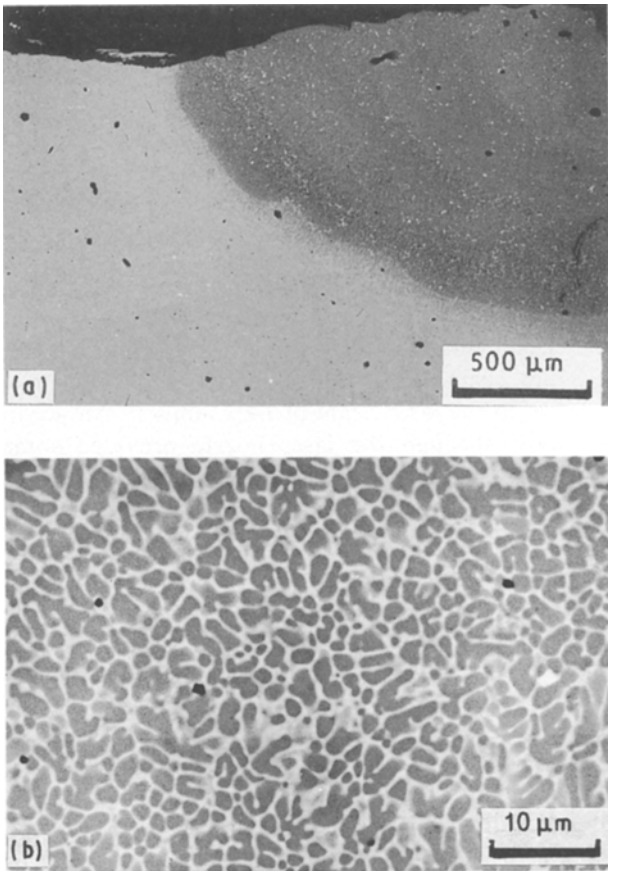

Figure 2 Single laser processed track of Al–10 wt % SiC mixture produced at 7.1 mm s^{-1} traverse speed, 4 g min^{-1} feed rate and 5 mm beam diameter: (a) low magnification of track and substrate, and (b) high magnification of the clad track.

TABLE II EDS analysis of Al–10 wt % SiC track produced at 7.1 traverse speed and 4 g min^{-1} feed rate (0.0094 g s^{-1} mass feed) (wt %)

Region	Ni	Al	Si	Cr	Mo	Fe	Nb	C
Average	17.0	49.1	1.4	17.9	7.9	3.2	3.0	0.5
Grey, dendrites	22.7	61.7	0.7	8.9	2.4	1.7	1.7	0.2
White, interdendritic	4.6	20.1	3.2	38.2	20.1	6.3	6.3	1.2

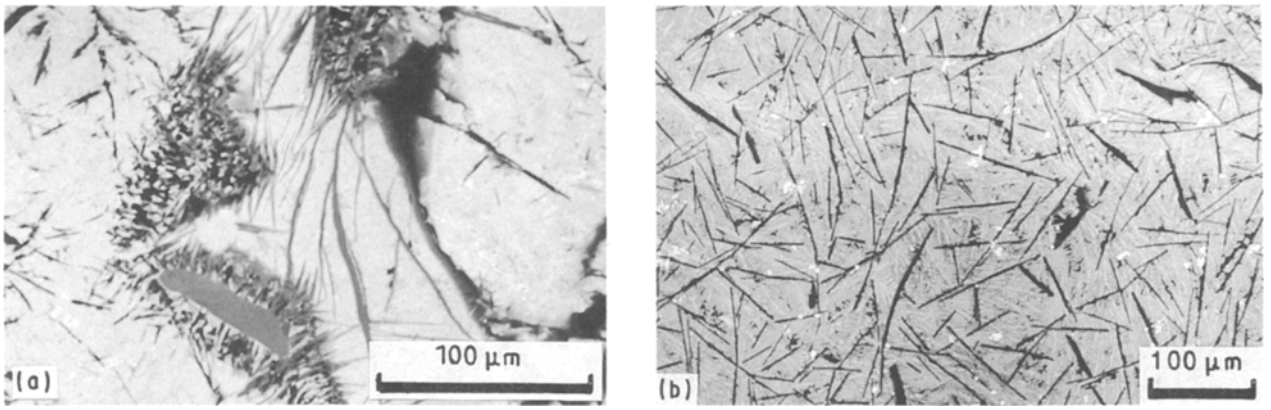

Figure 3 Some features of microstructures of single tracks of Al–10 wt % SiC produced at different laser conditions showing the presence of some undissolved SiC and Al_4C_3 (a) 6 g min^{-1} feed rate, 2.2 mm s^{-1} traverse speed and 2 kW laser power, and (b) 8 g min^{-1} feed rate, 3.9 mm s^{-1} traverse speed and 2 kW laser power.

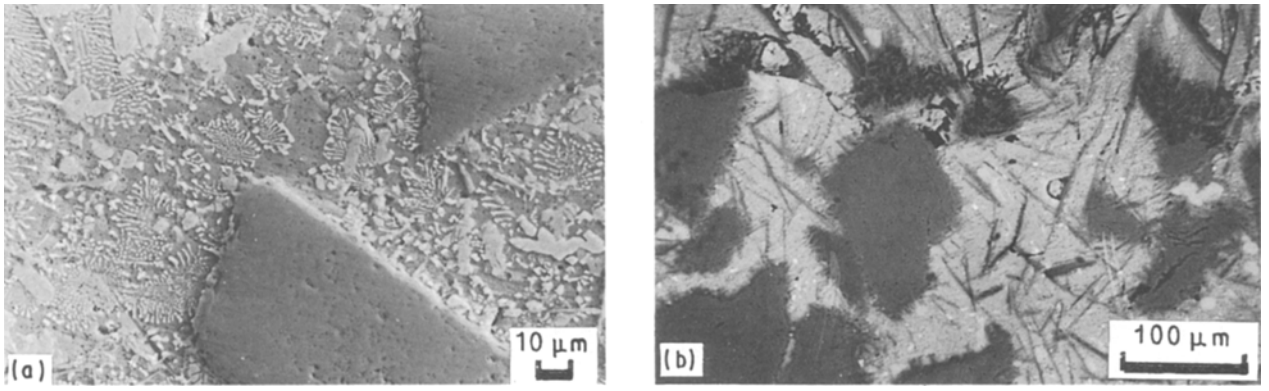

Figure 4 Some features of single tracks of Al–30 wt % SiC produced at different laser conditions: (a) 5 mm beam diameter, 7.1 mm s^{-1} traverse speed and 1.7 kW laser power, and (b) 3 mm beam diameter, 3.9 mm s^{-1} traverse speed and 2 kW laser power.

TABLE III EDS analysis of single track Al–30 wt % SiC, 7.1 mm s^{-1}, 5 mm s^{-1} traverse speed and 2 kW laser power (see Fig. 4a) (excluding undissolved SiC particles) (wt %)

Region	Ni	Al	Si	Cr	Mo	Fe	Nb	C
Eutectic (Al-rich)	7.9	90.3	0.5	0.4	0.2	0.3	0.2	0.2
Matrix	0.4	99	0.1	0.1	0.1	0.2	0.1	0
White (close to $NiAl_3$)	41.3	57	0.1	0.1	0.2	1.2	0.1	0
Grey (intermetallic)	4.4	69.7	1.0	14.9	8.0	0.8	0.8	0.4

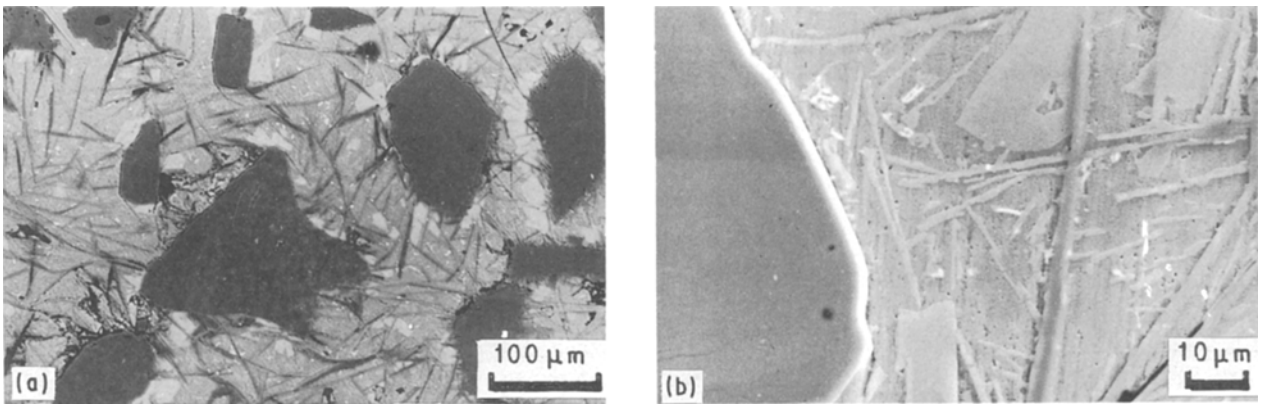

Figure 5 (a, b) Some features of microstructures of single track of Al–50 wt % SiC, 3.9 mm s^{-1} traverse speed, 5 g min^{-1} feed rate, 5 mm beam diameter and 2 kW laser power.

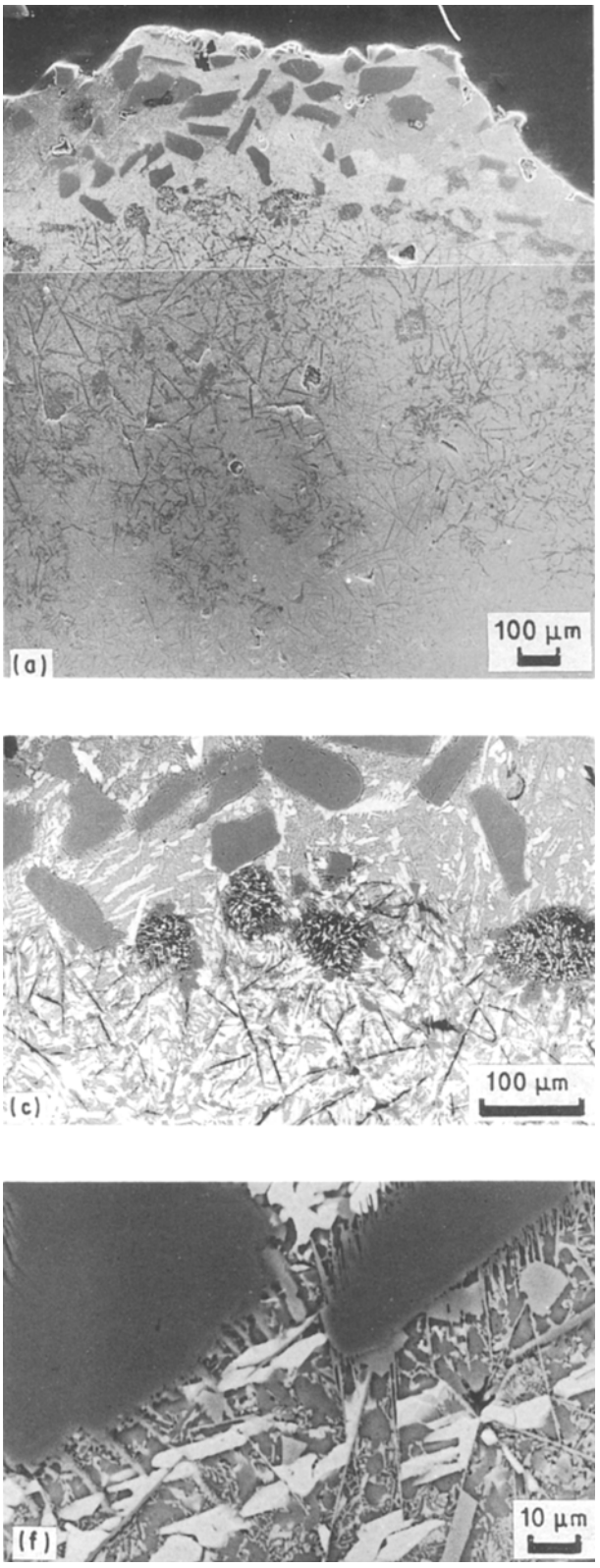

Figure 6 Microstructures of three fully overlapped tracks of aluminium containing 10, 30 and 50 wt % SiC: (a) general appearance, (b) high magnification of Al–10 wt % SiC, (c) interface of Al–10 wt % SiC and Al–30 wt % SiC, (d) high magnification of Al–30 wt % SiC, (e) Al–50 wt % SiC, and (f) high magnification of (e).

also achieved with the Al + 50 wt % SiC mixture (Fig. 5); the matrix showed a complex multiphase microstructure.

3.2. Functionally gradient materials

Fig. 6 illustrates the structure of a sample produced by three fully overlapped tracks at 3.9 mm s^{-1}, 5 mm beam diameter and feed rates of ~ 4, 5 and 5 g min^{-1} for the successive three tracks. Table IV gives average compositions of regions in tracks 1, 2 and 3, respectively. As might be expected the nickel, chromium, molybdenum and iron contents decrease and the aluminium content increases on going from track 1 to track 3, i.e. with increasing distance in the FGMs from the substrate. The silicon contents of tracks 2 and 3 are much higher than that of track 1, but the value for track 3 is lower than that of track 2 because of incomplete solution of SiC particles.

The microstructures vary in a complex way from the first track to the final track (Table V). The main feature to note is the complete or virtually complete

TABLE IV Average EDS analysis of overlapped FGM (see Fig. 6) (wt %)

Region	Ni	Al	Si	Cr	Mo	Fe	Nb	C
Track 1 (Al–10 wt % SiC)	45.4	27.9	4.9	11.9	4.9	1.0	2.0	2.0
Track 2, Al–30 wt % SiC	23.4	38.7	20.0	5.1	2.9	0.8	0.5	8.6
Track 3, Al–50 wt % SiC (no SiC included)	7.3	74.1	12.4	0.2	0.1	0.6	0.1	5.2

TABLE V EDS analysis of some features of overlapped tracks (Fig. 6) (wt %)

Region	Ni	Al	Si	Cr	Mo	Fe	Nb	C
Al–10 wt % SiC								
Near Substrate	46.1	27.6	4.8	11.7	4.8	1.0	2.0	2.0
100 μm from substrate	40.9	31.3	5.8	10.7	5.8	1.9	1.1	2.5
Interface 10/30 wt % SiC	33.6	34.1	13.7	7.8	3.1	1.0	1.0	5.7
Al–30 wt % SiC								
Matrix (point analysis)	0.2	98.1	0.8	0.2	0.1	0.2	0.1	0.3
White phase ($NiAl_3$)	44.4	54.1	0.1	0.2	0.1	1.0	0.1	0
Grey phase	3.9	70.2	1.0	16.2	7.5	0.8	0.1	0.3
Matrix + Al_4C_3	0.2	90.1	0.1	2.0	0.1	0.2	0.1	7.2
Al–50 wt % SiC								
White phase	46	52.0	0.2	0.2	0.5	1.0	0.1	0

solution of SiC particles in all but the surface region. Among other microstructural features are needle-like particles, interpreted by X-ray diffraction as Al_4C_3 in the central region of the FGM. In addition, the compositional data suggest that $NiAl_3$ is one of compounds formed; also particles of silicon are found in tracks 2 and 3. However, various other phases and constituents (including eutectics) are present, which have not been elucidated.

The simplified form of the multicomponent system can be represented schematically by considering nickel, aluminium, silicon and carbon as the main components and employing nickel, aluminium and SiC as the apexes on a ternary diagram (Fig. 7). A line joining SiC to aluminium contains the average compositions of the three powder mixtures, containing 10, 30, and 50 wt % SiC, respectively (positions 1, 2 and 3). The average compositions of the single tracks lie on lines joining points, 1, 2 and 3, respectively, to nickel, i.e. neglecting the alloying additions in the nickel alloy substrate. Thus, point (a) might represent the average composition of a track produced with Al–10 wt % SiC mixture. This figure also shows some of the phases that may form as reaction products, e.g. nickel aluminides. Compositions are controlled by the extent of dilution by nickel, which is a function of processing conditions, such as powder feed rate. When fully overlapping tracks are superimposed, the average compositions (including undissolved SiC) produced will derive from a combination of the compositions of the powder feed mixture and dilution from the previous tracks. For example, overlapping an Al–10 wt % SiC track with an Al–30 wt % SiC track will result in composition (b) on the diagram and a further overlap with Al–50 wt % SiC to composition c. The average matrix composition in cases where SiC particles are not fully dissolved will lie on extensions to the lines

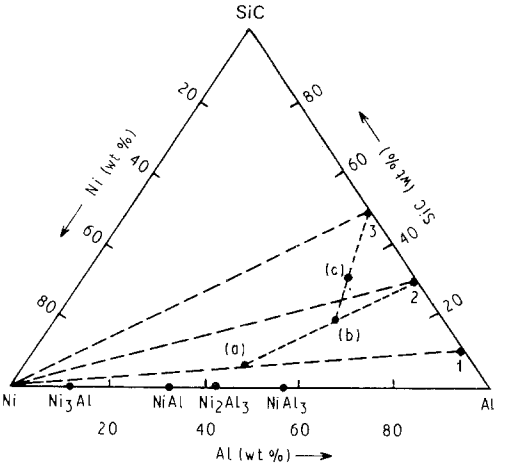

Figure 7 Ni–Al–SiC compositional triangle, from the Ni–Al–S–C phase diagram showing semi-schematically some compositional relationships of a functionally gradient material produced by overlapping three laser tracks (the effect of other elements in the substrate e.g. chromium, molybdenum, is neglected). (a), (b) and (c) indicate average compositions (including any undissolved SiC of laser tracks 1, 2 and 3, respectively).

joining points (a), (b) and (c) to SiC. Again these features depend sensitively on the process conditions. The assumption is made in the above statements that no preferential loss of any component occurs during processing.

The use of the four component system is a gross over-simplification of the situation where the substrate is a complex alloy such as IN 625. Full understanding of the constitution requires knowledge of the many intermediate phases that may form in the presence of the various alloy elements. Qualitatively it may be assumed that iron mainly enters into solid solution in nickel. Chromium and molybdenum may exercise their roles as carbide formers, and also appear in solution in nickel and participate in the formation

of intermediate phases based on nickel and/ or aluminium. Silicon may also be involved in compound formation and appear in elemental form.

4. Conclusions

With a mixture of Al and 10 wt % SiC, the range of processing conditions to achieve only partial solution of the SiC in an IN 625 substrate appears to be very limited. Also, depending on processing conditions, Al_4C_3, in needle-like morphology, forms as an undesirable phase in the matrix, as a result of carbon enrichment from the solution of SiC. With higher proportions of SiC, retention of the particles can be achieved more readily, but in the absence of substantial dilution from the substrate, the matrix becomes inappropriately high in aluminium; depending on the processing conditions a number of complex microstructure features can appear involving various phases (e.g. silicon and intermediate phases such as Al_4C_3).

In relation to the production of a functionally gradient material (FGM) by the laser processing of Al–SiC powder mixtures on a nickel alloy substrate (IN 625), it has been shown that three successive tracks can be deposited to give a wide range of compositions progressing from the inner to the outer regions. However, the accompanying changes in microstructure through the 3 mm thick FGM were not fully satisfactory. In particular, it was found to be difficult to retain a significant proportion of the SiC particles other than in the final layer of the FGM. Furthermore, because of the number of alloying additions in the substrate, the microstructures were complex and difficult to interpret. The results show the need for detailed consideration of the constitution when designing a multicomponent system and this paper has indicated how a ternary phase diagram may assist in this process.

Acknowledgements

We thank the SERC for financial support and INCO Alloys International for supplying the alloy substrate samples.

References

1. M. NINO and S. MAEDA, *ISIJ Int.* **30** (1990) 699.
2. K. ATARASHIYA, K. KUROKAWA, H. TAKAHASHI and H. MATSUI, *ibid.* **30** (1990) 1130.
3. T. HIRAI and M. SASAKI, *JSME Int*, **34** (1991) 123.
4. P. J. E. MONSON, W. M. STEEN and D. R. F. WEST, in "LASER advanced materials processing (LAMP 87)", (High Temperature Society of Japan and Japan Laser Processing Society, 1987) p. 377.
5. K. MOHAMMED JASIM, D. R. F. WEST, W. M. STEEN and R. D. RAWLINGS, in "Laser Materials Processing III", edited by J. Mazumder and K. Mukherjee (TMS-AIME, Warrendale, PA, 1989) p. 55.
6. K. MOHAMMED JASIM, R. D. RAWLINGS and D. R. F. WEST, *J. Mater. Sci.* **25** (1990) 4943.
7. J. D. AYERS, T. R. TUCKER and R. C. BOWERS, *Scripta Metall.* **14** (1980) 549.
8. J. D. AYERS, *Thin Solid Films* **84** (1981) 323.
9. J. D. AYERS and R. N. BOLLSTER, *Wear. Int.* **93** (1984) 193.
10. T. R. TUCKER, A. H. CLAUER, I. G. WRIGHT and J. T. STROPKI, *Thin Solid Films* **118** (1984) 73.
11. G. ABBAS, PhD thesis, University of London (1990).
12. J. A. FOLKES, PhD thesis, University of London (1986).
13. V. M. WEERASINGHE, PhD thesis, University of London (1984).
14. K. MOHAMMED JASIM and D. R. F. WEST, in "Laser and particle-beam chemical processing of surfaces", edited by A. W. Johnson, C. L. Loper and T. W. Sigmon (Materials Research Society, 1989) p. 139.

Received 29 June
and accepted 9 July 1992